Discover Geoscience

Research

Gamma-ray spectrometric evaluation in watersheds with gold anomalies in stream sediments, Passo Feio Complex, Caçapava do Sul region (Brazil)

Luiza Lima Alves[1] · César Augusto Moreira[1] · Ana Flávia da Silva Araújo[1] · Lenon Melo Ilha[2] · João Pedro Prado de Oliveira[1] · Sissa Kumaira[2] · Marco Antonio Fontoura Hansen[2] · Henri Masquelin[3]

Received: 12 March 2025 / Accepted: 26 May 2025
Published online: 05 June 2025

Abstract
This study utilizes gamma-ray spectrometry to identify source areas of gold recognized in geochemical prospecting work in stream sediments. The local geological context is represented by the Passo Feio Metamorphic Complex, which contains gold deposits possibly hosted in quartz veins concordant with metamorphic foliation, composed of quartzites, schists, and amphibolites. The study followed the sequence: geological reconnaissance, drone survey, and gamma-ray spectrometric acquisition. Field reconnaissance indicated an alternation of rocks oriented in a WNW/ENE direction, with recognition of quartz veins embedded concordantly with the foliation of quartzites. The drone data enabled the generation of a Digital Elevation Model (DEM) and served as a basis for planning the gamma-ray spectrometry work. A total of 715 gamma-ray spectrometric readings were taken, with an average spacing of 40 m between points, followed by data processing and the generation of maps of K (0.5–2.5%) concentrations, eU (0.9–3.9 ppm), and eTh (2.8–24.4 ppm). The data obtained regarding the K (%) concentration values reveal a clear anomaly in the central region with WNW/ENE orientation. The concentration data obtained for U (ppm) and Th (ppm) show a similar pattern concerning the WNW/ENE anomaly in the center of the area. The overlap of positive anomalies served as an indication of gold source areas in two river valleys. The combination of detailed gamma-ray spectrometry and precision digital terrain modeling has enabled the delineation of primary targets potentially mineralized in gold, in a versatile and fast way, compared to traditional soil sampling techniques.

Keywords Mineral exploration · Gold · Geophysics · Gamma-ray spectrometry

✉ Luiza Lima Alves, luiza.lima@unesp.br; César Augusto Moreira, cesar.a.moreira@unesp.br; Ana Flávia da Silva Araújo, af.araujo@unesp.br; Lenon Melo Ilha, lenonilha@unipampa.edu.br; João Pedro Prado de Oliveira, joao.pp.oliveira@unesp.br; Sissa Kumaira, sissakumaira@unipampa.edu.br; Marco Antonio Fontoura Hansen, marcohansen@unipampa.edu.br; Henri Masquelin, hmasquel@fcien.edu.uy | [1]Universidade Estadual Paulista "Júlio de Mesquita Filho", 24-A avenue, 1515, Bela Vista, Rio Claro, São Paulo 13506-900, Brazil. [2]Universidade Federal do Pampa, Campus Caçapava do Sul, Pedro Anunciação avenue, 111, Vila Batista, Caçapava do Sul, Rio Grande do Sul 96570-000, Brazil. [3]Instituto de Ciencias Geológicas, Universidad de la Republica, Iguá 4225 Esq. Mataojo, 11400 Montevideo, Uruguay.

1 Introduction

The exponential increase in demand for mineral resources has justified various research projects and the discovery of multiple mineral deposits in Brazil, activities that have driven economic growth and social development. The global market demands a wide variety of mineral commodities, making Brazil a major exporter on a global scale. Consequently, maintaining this activity depends on constant research and discoveries.

Gold is one of the oldest financial assets, offering high liquidity and security. It is widely used as a reserve during periods of international crises, leading to significant price increases on stock exchanges [1, 2]. In May 2024, the price of gold reached a historical record, with the ounce value climbing to $2,300, a significant increase compared to its average price of around $1,500 per ounce [2].

Gold consumption in Brazil has increased alongside the population's purchasing power, appearing in jewelry, electronic components for computers, tablets, notebooks, and mobile phones, as well as parts for the automotive industry, healthcare, dentistry, and even some construction components [3].

New mineral commodities are discovered through several progressive and inter-connected steps, which involve and predict increased investment and decreased risk [4, 5]. This process begins with the recognition of surface mineralization evidence, which may be associated with a subsurface ore body [5].

Geophysics is a highly mentioned tool in mineral exploration scenario for recognizing exploratory targets, since its field instruments allow for detecting contrasts between the physical properties of mineral deposits and their host rocks [6–11].

Gamma-ray spectrometry is a passive geophysical method, as it measures the in-herent radioactivity in the form of gamma rays from mineral species containing radi-oactive isotopes such as potassium (^{40}K), uranium (^{235}U e ^{238}U), and thorium (^{232}Th) [8]. This method enables rapid and easy data acquisition, allowing for extensive area coverage, though it is a shallow method with a maximum investigation depth of 50–100 cm [6, 8, 12]. Gamma-ray spectrometry offers several advantages in the analysis and quantification of elements in the soil compared to geochemical methods. In addition to the rapid acquisition of data, they can be easily processed using softwares, allowing results to be obtained shortly after the acquisition phase.

In mineral research, gamma-ray spectrometry is mainly applied to characteristically radioactive deposits, such as uranium, hydrothermal origin deposits or in soil samples [13–20]. Few references exist for studies related to gold deposits, primarily resulting from airborne geophysical surveys and remote sensing [21–27]. The mentioned gold exploration studies are based on airborne geophysical data and rely on sampling grids with wide spacing, typically with line intervals of approximately 1 km. As such, they are suitable for regional-scale investigations, often correlated with satellite imagery and enhanced through image processing techniques to highlight anomalous areas.

In contrast, the present study focuses on a relatively small watershed, emphasizing detailed ground gamma-ray spectrometry (with a 40-m spacing between sampling points) combined with the generation of high-resolution orthophotos acquired through drone surveys with centimeter-level accuracy. The primary objective is the development of a Digital Terrain Model (DTM) to support the spatial interpretation of potential geochemical halos (U, Th, and K). The innovation of this study lies in the use of a geophysical method capable of providing geochemical quantifications, supported by a high-precision digital terrain model, to identify potential primary sources of gold previously found in alluvial deposits.

2 Area location and history

The study area is located in the southernmost of Brazil, in the state of Rio Grande do Sul (RS). The occurrence studied is around 15 km from the urban area of the municipality of Caçapava do Sul, which is approximately 240 km from Porto Alegre, the state capital (Fig. 1).

Evidence of mineralization was recognized from regional studies carried out by the CPRM (Companhia de Pesquisa de Recursos Minerais, currently the Geological Service of Brazil) through the National Gold Prospecting Program in 2000, where geological reconnaissance and geochemical prospecting were carried out on stream sediments in an area of 136000 ha [28]. The regional geochemical survey for gold conducted by the Brazilian Geological Survey involved the analysis of a total of 818 stream sediment samples and 553 heavy mineral concentrate samples from alluvial material. The sampling stations were located at the mouths of drainages associated with metavolcanic-sedimentary lithologies, known for hosting various mineralizations in the studied region.

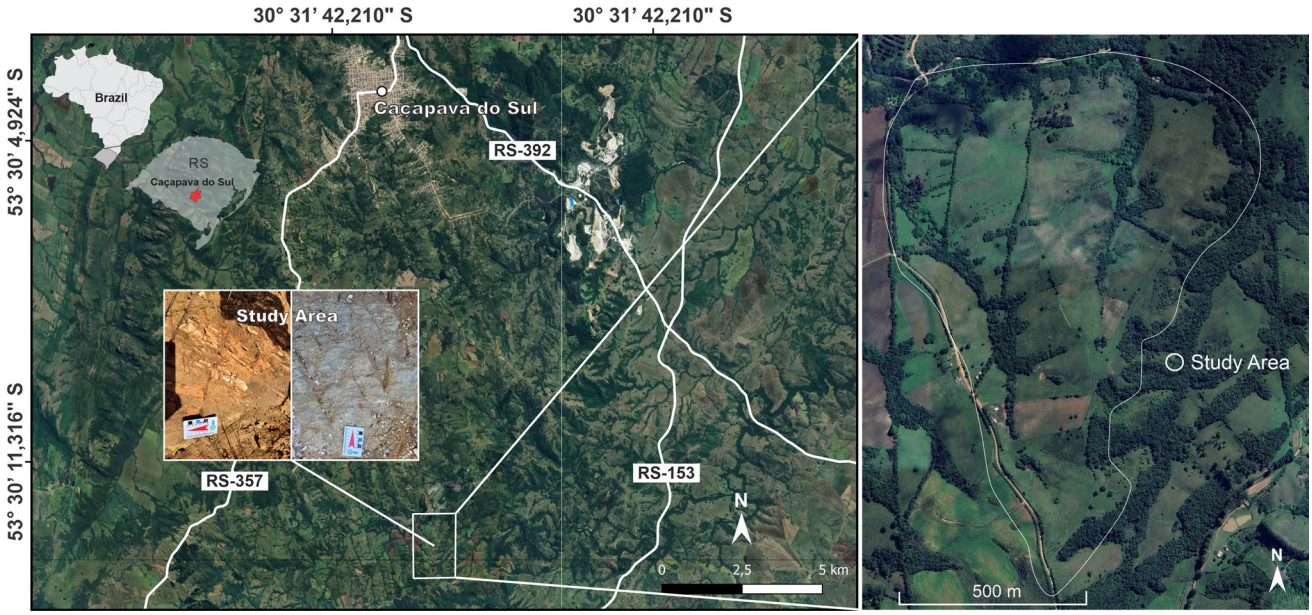

Fig. 1 Location of the study area in relation to Caçapava do Sul (RS)

At each station, a volume of 20 L of panned material was collected. The preparation and analysis of the samples for gold followed the routine below: (i) stream sediments were sieved to − 120 mesh, pulverized in the laboratory to − 200 mesh, and decomposed by fusion for analysis by plasma; (ii) heavy mineral concentrates were pulverized in the laboratory to − 200 mesh, decomposed by fusion, and analyzed by atomic absorption.

Two sub-basins with anomalous results for gold were selected as the target area for this study, based on the results of collecting samples of stream sediments and concentrates of heavy minerals in the alluvial material. There was a regional study on the area focused on defining anomalous basins, without detailing the origin of the gold [28]. Based on the hypothesis of weathering in outcropping deposits, followed by the transport of gold particles to the mouth regions of the basins, this work sought to follow the opposite path, based on an analysis of gamma-spectrometric data, in an attempt to recognize primary gold deposits in the study area. The decision to conduct the geophysical analysis using ground-based methods in the study area stemmed from a comparison with airborne methods, as the former allows for denser and more precise results.

Soil geochemical analysis is the most established and widely applied method for identifying anomalous halos in soils associated with mineralized zones [29–31]. Nonetheless, ground gamma-ray spectrometry represents a faster, more cost-effective, and operationally attractive alternative to conventional geochemical soil sampling, which requires laboratory analyses to obtain comparable results. Geophysical methods, in contrast, enable immediate data acquisition and interpretation. This study, therefore, highlights the applicability of gamma-ray spectrometry, particularly when integrated with the characteristic radioactive signature of low-sulfidation epithermal gold deposits.

3 Geology and metallogenetic origin

The study area encompasses rocks of the Caçapava do Sul Granitic Complex and the Passo Feio Metamorphic Complex, that are part of the igneous and metamorphic terrains that compose the Sul-Rio-Grandense Shield, formed during the Transamazonian (2.26–2.00 Ga) and Brasiliano (900–535 Ma) orogenic cycles [32].

The Caçapava do Sul Granitic Complex resulted from post-tectonic, calc-alkaline acidic magmatism, with its intrusion occurring at 562 ± 8 Ma during the late phases of the Brasiliano Orogeny evolution [28, 33]. Three granite rock facies are present: biotite granitoids, leucogranitoids, transitional granitoids, with crystals elongated in the N34W direction, the same as the metamorphic foliation of the Passo Feio Complex, which hosts the granitic complex [34].

The Passo Feio Metamorphic Complex consists of pelitic schists, phyllites, amphibolites, and metavolcanoclastic rocks and can be divided into a Metasedimentary Association and a Metavolcanic Association [28, 35]. It forms a doubly plunging antiform fold, with a sub-horizontal axis dipping towards NNE and SSW. The granitic complex intrudes its center, and

the unit serves as the basement for the Camaquã Basin [33, 36, 37]. Due to a scarcity of studies conducted in the area covered by the Metamor-phic Complex, the most detailed geological map available was made by the Geological Survey of Brazil, in a scale of 1:100.000 (Fig. 2).

The Metasedimentary Association is composed of metapelites and metavolcanoclastic rocks, represented by schists and phyllites containing muscovite, biotite, and/or chlorite, as well as minerals such as garnet, chloritoid, and staurolite. The foliation of these rocks is characterized by schistosity or slaty cleavage. The schist bands vary in thickness and are intercalated with amphibolites, quartz-feldspathic gneisses, and thin quartzite layers [35].

The Metavolcanic Association includes amphibolites, amphibole schists, amphibole gneisses, and massive amphibolites. These rocks exhibit planar and continuous structures with banding generated by metamorphic segregation or are massive [35].

The metapelites and amphibolites underwent two regional metamorphic events (M1 and M2) and three deformational phases (D1, D2, and D3), and among these, D3 is not associated with regional metamorphism [35, 38]. The D1 phase is preserved in quartz lenses, D2 formed the S2 foliation, and D3 created folds structuring the Passo Feio Metamorphic Complex.

The M1 event was characterized by the presence of minerals in the staurolite zone (amphibolite facies) and andalusite, indicative of a low-pressure event [34]. Metapelites and amphibolites are associated with M1, while M2 was a retrogressive event in the greenschist facies [34]. The Caçapava Granite intrusion occurred between the D2-M2 interval, with the S2 foliation of metamorphic rocks correlating with that of the granite. The ages of M1 and M2 were estimated at 685 ± 12 Ma and 562 ± 8 Ma, respectively [33].

The Passo Feio Metamorphic Complex hosts Cu (Au) and Pb mineralizations. The target of this study is a disseminated gold occurrence hosted in quartz veins concord-ant with the foliation of the host rock and associated with shear zones, with its para-genesis consisting of quartz, gold, pyrite, arsenopyrite, and chalcopyrite, classified as epigenetic hydrothermal deposits [28, 39].

The hydrothermal processes associated with the intrusion of the Caçapava do Sul Granitic Complex were responsible for the sulfide mineralization under study. Thermal fluids of magmatic origin mobilized metals from rocks adjacent to the Passo Feio Complex and deposited them in veins [33]. The deposits within the Metamorphic Complex are structurally controlled by NE-oriented strike-slip fault systems, formed during the Neoproterozoic collision processes involved in the formation of the Dom Feliciano Belt [40].

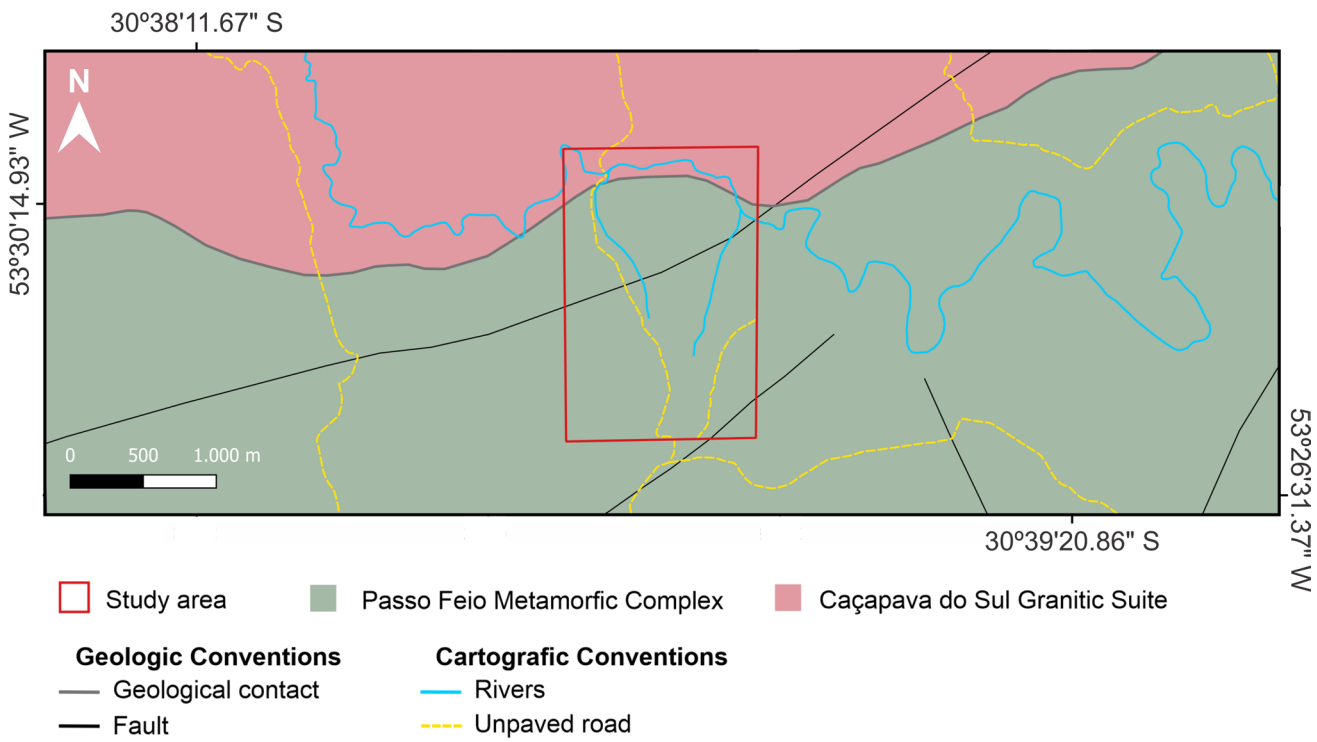

Fig. 2 Geological map (Modified from [21])

4 Methods

This study was conducted through geological reconnaissance, drone surveys for elaboration of Digital Elevation Model (DEM), and gamma-ray spectrometry investigation. The work began with the geological reconnaissance of the region, conducted in a N-S direction along a road that crosses orthogonally to the foliation present in the outcrops. Simultaneously, structural measurements of fractures and metamorphic foliations were collected to identify a possible direct or indirect relationship between the measured structures and the occurrence of gold.

Next, drone surveys were conducted using a DJI MAVIC 3 T model, where two flights were performed: one over the higher terrain and another over the lower terrain, with both flying at an altitude of 120 m (Fig. 3A). The drone flight lines were conducted in the E/W direction to ensure efficient coverage of the study area. The spatial resolution achieved was 20 cm, allowing for a detailed analysis of the terrain's topographic features.

The resulting images were combined using Agisoft Metashape software, which integrates the imported drone images. This process generated a digital point cloud that allowed for the measurement of altitude for each orthophoto. Through the interpolation of these altitude values, a Digital Elevation Model (DEM) was created.

Based on the results of the drone surveys and after a topographic analysis based on the DEM, the investigation area was delineated for geophysical surveying. The method employed was gamma-ray spectrometry, using the RS-332 Multipurpose Gamma-Ray Spectrometer System by Radiation Solutions Inc. This device offers high sensitivity, thermal protection, ease of use, and an integrated GPS (Fig. 5A). Additionally, the geophysical reading points were georeferenced using a differential GPS with 0.5 m precision.

The RS-332 measures the inherent radioactivity that occurs naturally in the form of gamma rays emitted by mineral species containing radioactive isotopes such as cosmogenic nuclides like potassium (^{40}K), uranium (^{235}U and ^{238}U), and thorium (^{232}Th). The spectrometer operates with a BGO (Bismuth Germanate Oxide) detector, that operates within a measurement range of 30–3000 keV. The Limit of Detection (LOD) of the RS-332 is determined by the combination of the measurement time, background conditions and the detector measurement range, in a way that longer sampling periods and higher background radiation can elevate the LOD.

The device's reading time can be configured as needed; for this study, it was set to 60 s. A study from 2014 determined that a 60 s reading time is reasonable for gamma-ray spectrometry analysis of volcanic rocks in the Paraná

Fig. 3 (**A**) Drone DJI MAVIC 3 T; (**B**) RS-332 with results on the screen after measurement on Point 44

Basin using a similar device [41]. Similarly, another one effectively used 60 s reading time to identify potential zones for acid mine drainage generation in uranium mine waste piles [42].

The spectrometer has a screen that allows real-time monitoring of the measurements obtained for each analyzed element at each point investigated (Fig. 3B). The elements U and Th are measured in ppm, while K is measured in percentage.

The selected area for data acquisition covered approximately 88 hectares, mostly covered by low vegetation and forests limited to drainage areas, with some points of exposed rock. Measurements were taken by directly placing the device on the surface of dry soil. Approximately 715 data points were collected, distributed in a regular grid at 40 m intervals, with differential GPS guidance in the field, which has an average error of 1 m.

After the data acquisition phase, processing was carried out using Geosoft's Oasis Montaj software to generate maps representing the radiometric distribution of eU, eTh, and K concentrations in the area. An interpolation of the collected data points was performed to create a two-dimensional representation of thorium, potassium, and uranium concentrations in terms of distance.

The interpolation process involved a least-squares approximation to smooth the discrepancies between field data and software-calculated values. A theoretical two-dimensional model was generated by segmenting the subsurface into rectangular blocks. The software automatically distributed and sized these blocks based on the data points' spatial distribution. The program calculates the concentrations based on the block model created from the comparison between the measured and modeled values, the parameters of these blocks are adjusted interactively until the apparent value agrees with the values acquired in the field.

The processed outputs were color-scaled maps representing each element's distribution, with potassium concentrations expressed as a percentage and eU and eTh concentrations in ppm. Additionally, ratio and ternary maps were generated and analyzed, however, they provided no further insights beyond those obtained from the original K, U, and Th maps.

5 Results and discussion

The mineralization in the study area has an epithermal hydrothermal character, which means it was formed at shallow depths. There are two types of mineralization that occur under these conditions: high- and low-sulfidation, with the latter occurring in the study area. In this case, the fluids associated with low-sulfidation deposits originate in zones of intense heat flow, where they reach equilibrium with the host rocks and exhibit a meteoric component, which may mix with magmatic fluids if active volcanism is nearby [43]. These deposits are typically formed in areas somewhat more distal from the volcanic center, as illustrated in the conceptual model in Fig. 4.

The concept of a geochemical dispersion halo was also considered for this study, since it represents an abnormally high or low concentrations of chemical elements that constitute a mineralization or associated alteration [44]. It is generated by the processes of mineral deposit formation through the introduction and/or redistribution of elements in the environment (primary geochemical halo) or formed by supergene processes (secondary geochemical halo) [44].

The initial stage of geological reconnaissance followed a N-S direction and revealed an alternation of rocks, varying between quartzites, schists and amphibolites, with a repetitive pattern across the explored area (Fig. 5B–D). Thus, it was expected that the geophysical data would show a standard pattern of alternation based on the local lithology, representing the area's background. Additionally, quartz veins were identified concordantly embedded in the quartzites' foliation, which are likely the hosts of the studied gold mineralization.

The drone flights produced a high-resolution orthophoto of the study area, superior to freely available satellite images, and a Digital Elevation Model (DEM) (Fig. 6). These data were initially analyzed from a geomorphological perspective and later integrated with gamma-ray spectrometry data to assess the geochemical mobility of the analyzed elements. The primary source of gold is likely outcropping, and weathering processes with destruction of mineralized rocks and veins, have resulted in the release of gold particles, which were carried to the basin's mouth. The elevation difference in the study area is 127 m, with the highest point in the southern portion (291 m) and the lowest in the Passo Feio River region (164 m).

The gamma-ray spectrometric acquisition was conducted alongside differential GPS surveying. This equipment provides more precise coordinates than the GPS integrated into the RS-332, with a margin of error of only 0.5 m, that provided a better result for the regular grid of 40 m intervals. Thus, it enabled the creation of the point map for gamma-ray spectrometry analysis (Fig. 7).

This study began interpreting the data using the altimetry values obtained from the DEM. These values were analyzed concerning terrain morphology, weathering, and element mobility in the geological environment, as these factors are

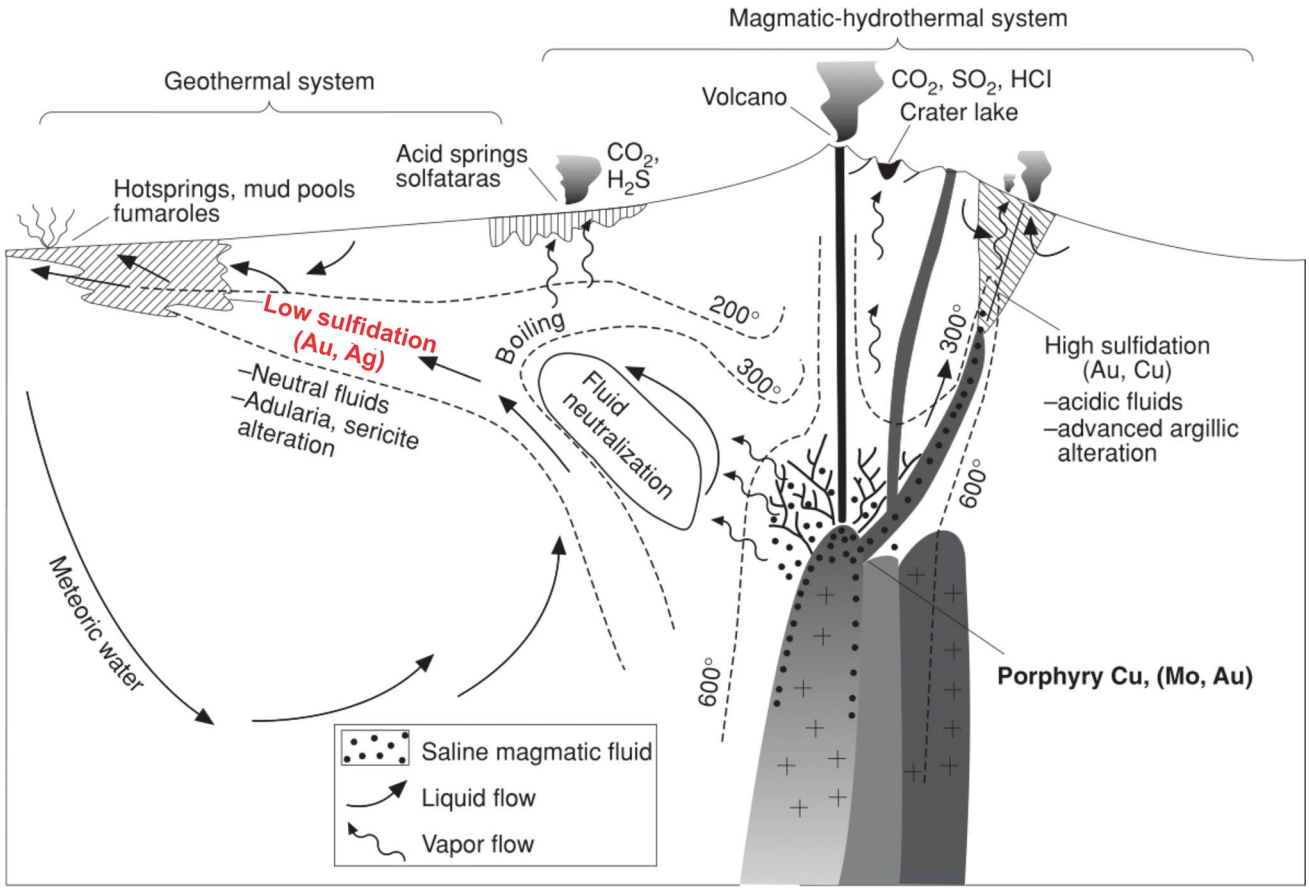

Fig. 4 The geological setting and characteristics of high-sulfidation and low-sulfidation deposits. [modified from 43]

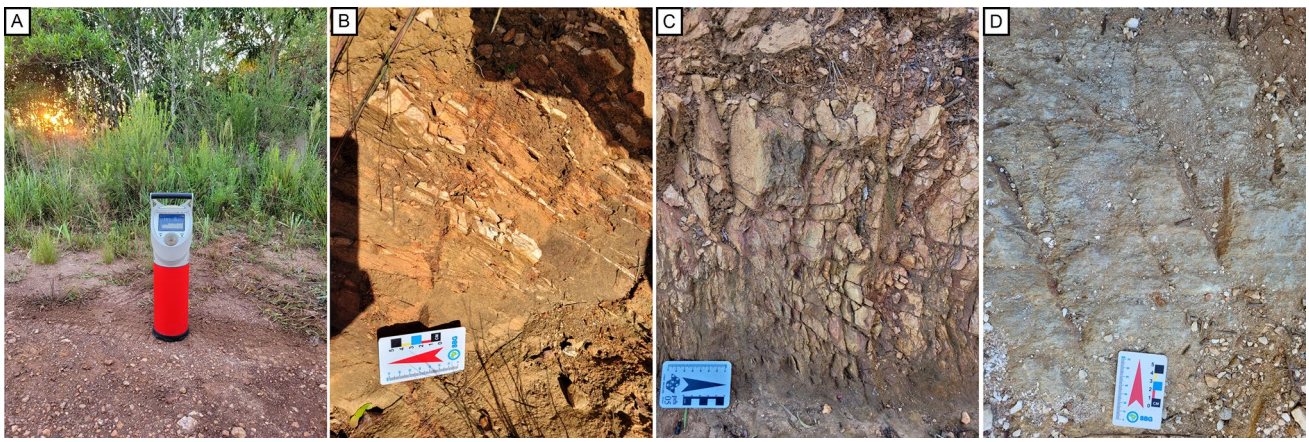

Fig. 5 (**A**) RS-332 conducting a measurement. (**B**) Quartzites with quartz veins embedded in metamorphic foliation. (**C**) Schists (**D**) Amphibolites

crucial for assessing radioelement distribution at the Earth's surface. Naturally, sediment transport caused by erosion and physical weathering moves materials from higher elevations to lower areas, such as rivers floodplains. Geochemical element mobilization occurs through leaching and hydrothermal fluid activity, following the same patterns of movement as discussed before [45–47].

Potassium (K) is a lithophile, incompatible (especially during magma crystallization), and volatile element with high environmental mobility, primarily occurring in granitoids [46, 48]. Uranium (U) becomes mobile under hydrothermal and

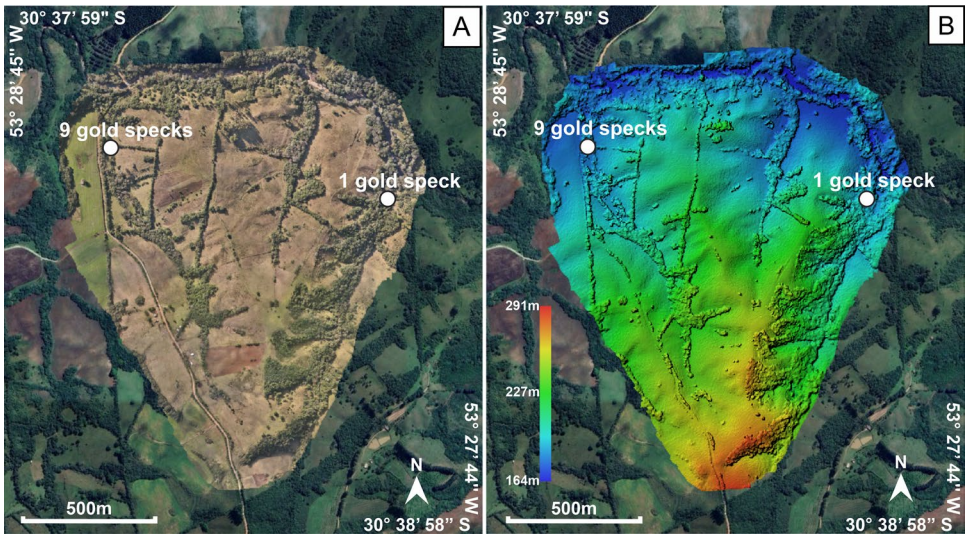

Fig. 6 Products from drone surveys and locations of [21] sampling points, showing the number of gold specks found in stream sediments. (**A**) Orthophoto of the study area. (**B**) DEM of the study area

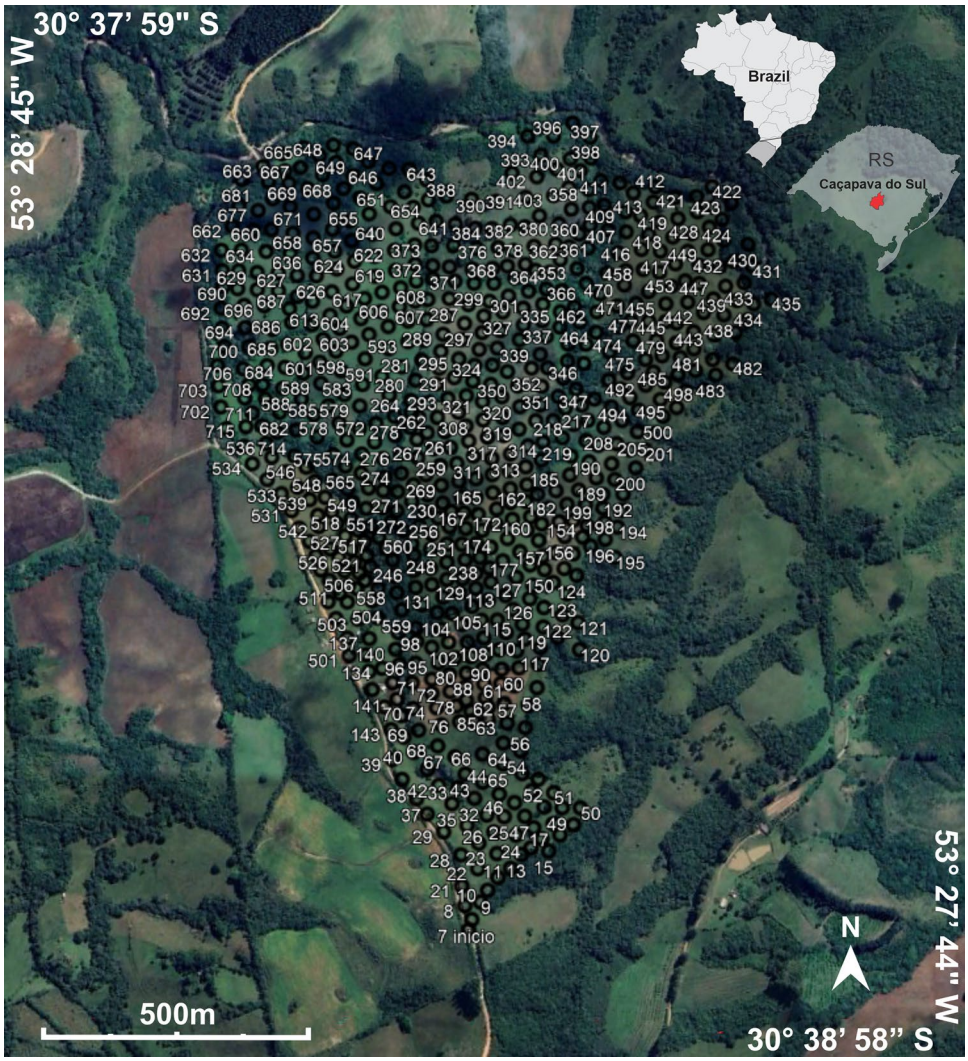

Fig. 7 Point map for gamma-ray spectrometry

supergenic conditions [46, 48]. Thorium (Th) is less abundant in the crust and typically measured in ppb or ppm [46, 49]. The chemical fractionation of U and Th series members occurs during magmatic processes [48].

Geomorphology, weathering, erosion, and the source rock collectively control the radioelement distribution in surface materials, creating differences from the bedrock background. Processes include K depletion during soil formation, K and Th enrichment through silicification in schists, and reduced K values during schist pedogenesis [46]. Generally, radioelement mobilization varies based on ground-water flow and leaching, with K being significantly more mobile than U or Th in such scenarios [50]. A study characterized various mineral deposits using airborne gamma-ray spectrometry, including gold mineralization in metavolcanic/metasedimentary rocks with hydrothermal alteration (K enrichment), which resembles the present study area [51].

Potassium concentrations, expressed as percentages (%), ranged from 0.5 to 2.5% (Fig. 8A). A noticeable anomaly with high concentrations (1.2–2.5%) is present in the central region, oriented NE/SW, coinciding with the schists' metamorphic foliation direction. This area has undergone hydrothermal alteration due to the intrusion of the Caçapava do Sul Granitic Complex. Potassium is present in the micas forming the schists; therefore, potassium anomalies were associated with the schist lithotype. Additionally, a high K concentration area is evident in the northern region (Fig. 8A).

Uranium (U) and thorium (Th) concentrations, expressed in ppm, ranged from 0.9 to 3.9 ppm for U and 2.8–24.4 ppm for Th (Fig. 8B, C). Compared to the K values, both show anomalies with a NE/SW orientation positioned in the central region of the area, however, the anomalous areas are not superimposed, with the eU and eTh anomalous areas shifting northwards (Fig. 8D). U and Th originate exclusively from hydrothermal processes, as they are more abundant in the mantle and concentrated in the crust through magma ascent [45]. In the study area, this correlates with the regional hydrothermal event responsible for mobilizing U and Th and their subsequent deposition in mineralized quartz veins

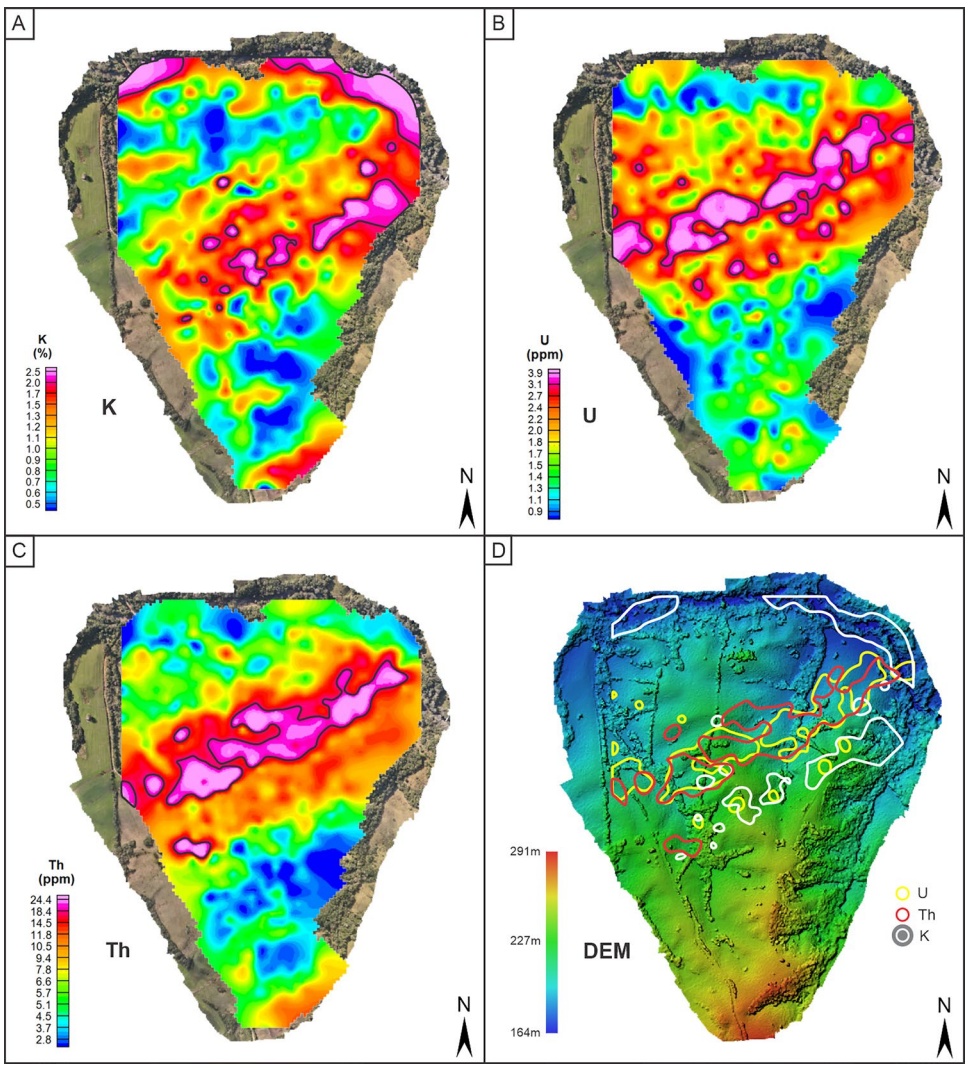

Fig. 8 (**A**) 2D interpolation map of K concentration, with the areas with the highest values highlighted in black. (**B**) 2D interpolation map of U concentration, with the areas with the highest values highlighted in black. (**C**) 2D interpolation map of Th concentration, with the areas with the highest values highlighted in black. (**D**) Areas with the highest element concentration values superimposed on the DEM

embedded in metamorphic foliation. In this sense, U and Th exist only in the veins generated by the hydrothermal processes that are hosted within the quartzites, making them directly associated with the gold mineralization, and serving as a prospecting guide in the study area.

An integrated analysis of K, U, and Th maps reveals differences in each element's dispersion halos on the surface. In terms of mobility, K is the most mobile, U is intermediate, and Th is the least mobile under weathering processes. Soil thickness is a critical factor for element mobility, as greater thickness allows higher K, U, and Th concentrations to become available for mobilization. Geological reconnaissance revealed underdeveloped soils (up to 30 cm thick) rich in rock fragments at several points. Under such conditions, gamma-ray spectrometry anomalies primarily reflect signatures associated with the underlying rocks, whether related to original mineral composition or hydrothermal processes.

Two high K concentration regions or dispersion halos are evident. The Passo Feio River lies within a regional watershed, so the K anomaly in the floodplain consists of the sedimentation of fine suspended particles, predominantly clay minerals, may result from weathering in the study area's rocks or external factors, including the Caçapava do Sul Granitic Complex weathering.

For U, the highest concentration (3.1–3.9 ppm) is central, with some dispersion around it. Th shows a smaller dispersion halo with higher values (14.5–24.4 ppm), potentially representing or delineating a zone with gold mineralization in quartz veins.

To integrate the data, a map of anomalous halos for each element was generated and overlaid onto the DEM (Fig. 8D). There is a coincidence between U and Th anomalies, with an absence of K in this domain, suggesting quartz vein emplacement in quartzites, which contain less K. Conversely, the K anomaly upstream of the U and Th halos may be associated with hydrothermalism in schists, a lithotype without quartz veins and likely barren of gold. Furthermore, the overlap of the anomalous halos proved effective in highlighting that they all share the same NE/SW orientation, consistent with the regional structural trend. This orientation aligns with the foliation of the rocks, quartz veins, fractures, and regional faults.

The regional gold occurrences consist of quartz veins aligned concordantly with the foliation of the lithologies of the Metavolcanic-Sedimentary Belts, represented in the study area by the Passo Feio Metamorphic Complex [52]. There are several small prospects and deposits associated with the Caçapava do Sul Granitic Complex, hosted in the Passo Feio rocks, which include Cu (Au) and Pb sulfide veins of an epigenetic hydrothermal origin [33]. As discussed in [33], the region lacks prior studies, so the origin of the metal present in the mineralizing fluids of these deposits has not yet been investigated.

Thus, the mineralizations hosted in the metasediments of the Passo Feio Meta-morphic Complex are associated with a remobilization or reconcentration of metallic elements, likely derived from adjacent rocks. The intrusion event of the Caçapava do Sul Granitic Complex resulted in local metamorphism and was responsible for providing the hydrothermal fluids that caused this remobilization and their deposition in the quartz veins. These veins were positioned along weakness planes, represented by the foliation and regional fractures, which have a NE/SW orientation.

6 Conclusions

Studies describing the metallogeny of gold in the study region suggest a magmatic/hydrothermal origin, although the Caçapava do Sul Granitic Complex is barren for gold it was responsible for the last regional deformation of the Passo Feio Complex rocks that concentrated gold in the quartz veins.

Although gamma spectrometry is widely used in mineral prospecting for the identification of radioactive deposits, this study highlights the application of the method for a hydrothermal-origin gold deposit. The association of U and Th with mineralization provides a new perspective for identifying potentially gold-bearing areas, in other words, the study presents an innovative application of ground gamma-ray spectrometry, as it allows for a broad and detailed survey of areas with mineral potential, enabling the delineation of sampling and grade analysis targets in a rapid and cost-effective manner.

The elements U and Th are related to hydrothermal processes and the surface anomalies of high values obtained coincide with the mineralized quartz veins. In this sense, quartzites represent the main lithotype or regional prospecting guide for gold searches.

The sampling grid for gamma-ray spectrometry was sufficient to detect the geochemical halos of U, Th, and K, which, when analyzed together with the digital terrain model has satisfactorily delimited potentially gold-mineralized targets, contained in a strip that crosses the two sub-basins recognized as anomalous in the geochemistry of stream sediments, and the probable primary outcropping source of gold.

Acknowledgements The authors are especially grateful to the Fundação de Amparo à Pesquisa do Estado de São Paulo—FAPESP for funding the field trip of the Project. We also would like to thank the Coordenação de Aperfeiçoamento de Pessoal de Nível Superior (CAPES) for financial support on the masters' scholarship of Luiza Lima Alves. We are also thankful for the support provided by Universidade Federal do Pampa, Campus de Caçapava do Sul – UNIPAMPA.

Author contributions Author Contributions: Conceptualization: L.L.A and C.A.M; Methodology: L.L.A and C.A.M; Software: L.M.I.; Investigation: L.L.A., C.A.M., A.F.S.A., L.M.I., S. K., M.A.F.H., J.P.P.O., H.M.; Writing—original draft preparation: L.L.A.; Preparation of figures: L.L.A., C.A.M, J.P.P.O.; Writing—review and editing, L.L.A., J.P.P.O., C.A.M.; Supervision, C.A.M.; Project administration, C.A.M. and H.M.; All authors reviewed the manuscript.

Funding This research was funded by FAPESP—Fundação de Amparo à Pesquisa do Estado de São Paulo (Process n. 2023/04732–8).

Data availability The data generated and analyzed, that supports the findings of this study, are not publicy available, but are available from the corresponding author on reasonable request.

Declarations

Ethics approval and consent to participate Not applicable.

Consent to publication Not applicable.

Competing interests The authors declare no competing interests.

References

1. IBRAM – Instituto Brasileiro De Mineração. Informações e Análises da Economia Mineral Brasileira, 2012. Available online: https://ibram.org.br/wp-content/uploads/2020/12/informacoes-sobre-a-economia-mineral-2017.pdf (Acessed on 30/06/2024).
2. KITCO. Gold Price Today. Available online: https://www.kitco.com/gold-price-today-usa/ (Acessed on 10/07/2024).
3. World Gold Council. 2024. Available online: https://www.gold.org/ (Acessed on: 05/11/2024).
4. Moon CJ, Whateley MK, Evans AM. Introduction to mineral exploration. 2nd ed. Hoboken, United States: Blackwell Publishing; 2006.
5. Marjoribanks R. Geological methods in mineral exploration and mining. 2nd ed. Heidelberg, Germany: Springer; 2010.
6. Mussett AE, Khan MA. Looking into the earth: an introduction to geological geophysics. 1st ed. New York, United States: Cambridge University Press; 2000.
7. Ford K, Keating P, Thomas MD. Overview of geophysical signatures associated with Canadian ore deposits. In: Goodfellow WD, editor. Mineral deposits of canada: a synthesis of major deposit-types, district metallogeny, the evolution of geological provinces, and ex-ploration methods. Canada: Geological Association of Canada, Mineral Deposits Division, Special Publication; 2007. p. 939–70.
8. Dentith M, Mudge ST. Geophysics for the mineral exploration geoscientist. 1st ed. New York: Cambridge University Press; 2014. p. 1–438.
9. Lu DB, Wang F, Chen XD, et al. An improved ERT approach for the investigation of subsurface structures. Pure Appl Geophys. 2017;174:375–86. https://doi.org/10.1007/s00024-016-1386-9.
10. Kühn C, Brasse H, Schwarz G. Three-dimensional electrical resistivity image of the Volcan-ic Arc in Northern Chile—an appraisal of early magnetotelluric data. Pure Appl Geophys. 2017;175:2153–65. https://doi.org/10.1007/s00024-017-1764-y.
11. Zhang G, Lü QT, Zhang GB, Lin PR, Jia ZY, Suo K. Joint interpretation of geological, magnetic, AMT, and ERT data for mineral exploration in the northeast of inner mongolia, China. Pure Appl Geophys. 2017;175:989–1002. https://doi.org/10.1007/s00024-017-1733-5.
12. Milsom J. Field geophysics. The geological field guide series. 3rd ed. London: University College London; 2003. p. 1–232.
13. Shives RBK, Charbonneau BW, Ford KL. The detection of potassic alteration by gamma-ray spectrome-try—recognition of alteration related to mineralization. Geophysics. 2000;65(6):2001–11. https://doi.org/10.1190/1.1444884.
14. Gaafar I. Application of gamma ray spectrometric measurements and VLF-EM data for tracing vein type uranium minerali-zation, El-Sela area, South Eastern Desert, Egypt. NRIAG J Astron Geophys. 2015;4(2):266–82. https://doi.org/10.1016/j.nrjag.2015.10.001.
15. Elkhadragy AA, Ismail AA, Eltarras MM, Azzazy AA. Utilization of airborne gamma ray spec-trometric data for radi-oactive mineral exploration of G.Abu Had—G.Umm Qaraf area, South Eastern Desert, Egypt, NRIAG. J Astron Geophys. 2017;6(1):148–61. https://doi.org/10.1016/j.nrjag.2016.12.001.
16. Alhumimidi MS, Aboud E, Alqahtani F, Al-Battahien A, Saud R, Alqahtani HH, Aljuhani N, Alyousif MM, Alyousef KA. Gamma-ray spectrometric survey for mineral exploration at Baljurashi area, Saudi Arabia. J Radiat Res Appl Sci. 2021;14(1):82–90. https://doi.org/10.1080/16878507.2020.1856600.

17. Beogo CE, Cisse OI, Ansong M, Zougmore F. Gamma-ray spectrometry of soil samples from a pilot site of uranium anomaly in the Sahel region of Burkina Faso. Appl Environ Soil Sci. 2024. https://doi.org/10.1155/aess/9229457.
18. Ekwok SE, et al. Unveiling the mineral resources and structural patterns in the middle benue trough: a comprehensive exploration using airborne magnetic and radiometric data. Geocarto Int. 2024. https://doi.org/10.1080/10106049.2024.2339290.
19. Hegab MAER. A multi-disciplinary approach for uranium exploration using remote sensing and airborne gamma-ray spectrometry data in the Gebel Duwi area, Central Eastern Desert, Egypt. Sci Rep. 2024;14:19739. https://doi.org/10.1038/s41598-024-69147-3.
20. Hegab MAER, Magd IAE, Wahid KHAE. Revealing potential mineralization zones utilizing landsat-9, ASTER and airborne radiometric data at elkharaza-Dara area, north eastern desert, Egypt. Egypt J Remote Sens Space Sci. 2024;27(4):716–33. https://doi.org/10.1016/j.ejrs.2024.10.005.
21. Maden N, Enver A. Gamma ray spectrometry for recognition of hydrothermal alteration zones related to a low sulfi-dation epithermal gold mineralization (eastern Pontides, NE Türki-ye). J Appl Geophys. 2015;122:74–85.
22. Pereira BM, Ferreira J. Recognition of gold mineralization favorability zones through airborne gamma-ray spectrometry and magnetometry in brusque and Botuverá Region, Southern Bra-zil. Bra J Geophys. 2018;36(3):361–361.
23. Shebl A, Abdellatif M, Elkhateeb SO, Csámer Á. multisource data analysis for gold potenti-ality mapping of Atalla area and its environs, central Eastern Desert, Egypt. Minerals. 2021;11(6):641. https://doi.org/10.3390/min11060641.
24. El-Sadek MA. Using of airborne gamma-ray spectrometric data to the exposure of potassic alteration -recognition of alteration relates to gold mineralization. Appl Radiat Isot. 2022;190:389–403. https://doi.org/10.1016/j.jafrearsci.2017.07.012.
25. Saleh A, Salako KA, Salawu NB, et al. Airborne magnetic and gamma-ray spectrometric pro-specting to delineate structures associated with gold mineralization—a case study in Yauri region, Northwestern, Nigeria. Arab J Geosci. 2023;16:308. https://doi.org/10.1007/s12517-023-11380-7.
26. Hegab MA. Remote sensing and gamma-ray spectrometry based gold related alteration zones detection: case study (Um Balad area), North Eastern Desert, Egypt. Pure Appl Geophys. 2021;178:3909–31. https://doi.org/10.1007/s00024-021-02865-1.
27. Hegab MAE-R, Mousa SE, Salem SM, Farag K, GabAllah H. Gold-related alteration zones detection at the um balad area, Egyptian eastern desert, using remote sensing, geophysical, and GIS data analysis. J Afr Earth Sci. 2022;196(104715):104715. https://doi.org/10.1016/j.jafrearsci.2022.104715.
28. CPRM – Companhia de Pesquisa de Recursos Minerais. Programa Nacional de Prospecção de Ouro. Resultados da prospecção para ouro na área RS-01 Lavras do Sul/Caçapava do Sul, Subárea Caçapava do Sul, Rio Grande do Sul. Porto Alegre. 2000. 14p. https://rigeo.sgb.gov.br/handle/doc/1589.
29. Kyser K, Barr J, Ihlenfeld C. Applied geochemistry in mineral exploration and mining. Elements. 2015;11(4):241–6. https://doi.org/10.2113/gselements.11.4.241.
30. Grunsky EC, de Caritat P. State-of-the-art analysis of geochemical data for mineral exploration. Geochem: Explor, Environ, Anal. 2020;20(2):217–32. https://doi.org/10.1144/geochem2019-031.
31. Dönmez H. Applications of soil geochemistry in mineral exploration. 2023. Zenodo. https://doi.org/10.5281/ZENODO.10436738.
32. Soliani Junior E, Kawashita K, Baitelli R. A Geologia Isotópica do Escudo Sul-rio-grandense—Parte I: métodos isotópicos e valor interpretativo. In: Holz M, Deros LF, editors. Geologia do rio grande do sul. 1st ed. Porto Alegre: Universidade Federal do Rio Grande do Sul; 2000. p. 161–74.
33. Remus MVD, Hartmann LA, Mcnaughton NJ, Groves DI, Fletcher IR. The link be-tween hydrothermal epigenetic copper mineralization and the Caçapava Granite of the Brasiliano Cy-cle in Southern Brazil. J S Am Earth Sci. 2000;13(3):191–216. https://doi.org/10.1016/S0895-9811(00)00017-1.
34. Nardi LVS, Bitencourt MF. Geologia, petrologia e geoquímica do Complexo Granítico de Caçapava do Sul, RS. Revista Brasileira de Geociências. 1989;19(2):153–69.
35. Bitencourt, M. F. Metamorfitos da região de Caçapava do Sul, RS – Geologia e Relações com o Corpo Granítico. In: Atas do 1º Simpósio Sul-Brasileiro de Geologia. 1983a. pp. 37–48
36. Paim PSG, Chemale F Jr, Wildner W. Estágios evolutivos da Bacia do Camaquã (RS). Ciência e Natura, Santa Maria. 2014;36:183–93.
37. da Costa EO, Bitencourt MF, Tennholm T, Konopásek J, Moita T. De F. P-T-D evolution of the southeast Passo Feio complex and the meaning of the Caçapava lineament, Dom Feliciano Belt, southernmost Brazil. J South Am Earth Sci. 2021;112(1):103465. https://doi.org/10.1016/j.jsames.2021.103465.
38. Bitencourt, M. F. Geologia, Petrologia e Estrutura do Metamorfitos da Região de Caçapava do Sul, RS. Master Thesis, Programa de Pós-Graduação em Geociências, Instituto de Geociências, Univer-sidade Federal do Rio Grande do Sul, Porto Alegre, Brazil, 1983b.
39. Toniolo JA, Gil CAA, Sander A. Projeto Baneo—metalogenia das bacias neoproterozóico-eopaleozóicas do Sul do Brasil, Bacia do Camaquã. Porto Alegre: Serviço Geológico do Brasil; 2007. p. 138.
40. Ribeiro M, Bocchi PR, Figueiredo Filho PM, Tessari RI. Geologia da quadrícula de Caçapava do Sul, RS, Brasil. Boletim da Divisão de Geologia e Mineralogia, DPM-DNPM. 1966;127:1–232.
41. Nardy AJR, Moreira CA, Machado FB, Luchetti ACF, Hansen MAF, Rossini AR, Barbosa V Jr. Gamma-ray spectometry signature of paraná volcanic rocks: preliminary results. Geociências. 2014;33(2):216–27.
42. Marques ACG, Moreira CA, Casagrande MFS, Arcila EJA. Gamma-ray spectrometry applied in the identification of potential acid mine drainage generation zones in waste rock pile with uranium ore and associated sulfides (Caldas, Brazil). Geofísica Int. 2022;61(3):251–66. https://doi.org/10.2220/igeof.00167169p.2022.61.3.2207.
43. Roob L. Introduction to ore-forming processes. Oxford: Blackwell; 2005.
44. Licht OAB. Prospecção geoquímica: princípios, técnicas e métodos. Rio de Janeiro: Companhia de Pesquisa de Recursos Minerais—CPRM; 1998. p. 236.
45. Mcsween HY, Richardson SM, Uhle ME. Geochemistry: pathways and processes. New York: Columbia University Press; 2003. p. 363.
46. Gilmore G. Practical gamma-ray spectrometry. United Kingdom: John Wiley & Sons Ltd; 2008. p. 387.
47. Macheyeki AS, Li X, Kafumu DP, Yuan F. Applied geochemistry: advances in mineral exploration techniques. Amsterdam, Netherlands: Elsevier Inc.; 2020. p. 210.

48. International Atomic Energy Agency (IAEA). Guidelines for radioelement mapping using gamma ray spectrometry data. Viena, Áustria, 2003. 172p.
49. Dickson BL, Scott KM. Interpretation of aerial gamma ray surveys-adding the geochemical factors. J Aust Geol Geophys. 1997;17(2):187–200.
50. Wilford JR, Bierwirth PN, Craig MA. Application of airborne gamma ray spectrometry in soil/regolith mapping and applied geomorphology. J Aust Geol Geophys. 1997;17(2):201–16.
51. Shives, R.B.K.; Ford, K.L.; Charbonneau, B.W. Geological Survey of Canada Workshop Manual: Applications of Gamma ray Spectrometric/Magnetic/VLF-EM Surveys. Geological Survey of Canada. 1995. Open File 3061, pp. 85.
52. PORCHER, C. A.; LEITES, S. R.; RAMGRAB, G. E.; CAMOZZATO, E. Passo do Salsinho, Folha SH.22-Y-A-I-4, Estado do Rio Grande do Sul. Brasília: Companhia de Pesquisa de Recursos Minerais – CPRM, 1995. (Programa Levantamentos Geológicos Básicos do Brasil).